

Hussam Raad¹, Emad Kadum Njim², Muhsin J. Jweeg³, Muhannad Al-Waily¹

Sandwiched Plate Vibration Analysis with Open and Closed Lattice

¹*Department of Mechanical Engineering, Faculty of Engineering, University of Kufa, Iraq*

²*Ministry of Industry and Minerals, State Company for Rubber and Tires Industries, Iraq*

³*Al-Farahidi University, College of Technical Engineering, Iraq*

This work attempts to replace the sandwich core's traditional shape and material with a cellular pattern, where the cells have a regular shape, distribution, and size. The contribution of this paper is to design two structures, one open-celled and the other closed, and to evaluate the performance of sandwich plates with lattice cell core as it is used for many industrial applications, particularly in automobile engineering. The new theoretical formulations are constructed for two structures to find the free vibration characteristics. The results of the new design are compared with the traditional shape. Derivation of equations to predict mechanical properties based on relative density with the chosen shapes, specific vibration equation of three-layer sandwich plate, and substitution by equation using excel sheet. Results are promising, and the effectiveness of cellular pattern theoretical analysis estimation. Limitations and error rates for the mechanical properties come through the empirical equations, and their ratio to the relative density values are higher depending on the behavior of the core material. Findings reveal, with open cell decrease in modulus of elasticity by (PLA: -90.4%) and (TPU: -90.4%), increases natural frequency by (PLA: 44.5%) and (TPU: 46.4%), as for closed-cell decreases in the modulus of elasticity by (PLA: -66.9%) and (TPU: -64.4%), increases natural frequency by (PLA: 36%) and (TPU: 37.7%). Converting a solid substance or replacing a foam form with a cellular pattern is one way to better performance and save weight through the selected cell pattern in absorbing the energy of the vibration wave.

Keywords: sandwich plate, free vibration, lattice structural, strut section, closed and open cell, relative density.

Received 17 November 2022; accepted 8 June 2023.

Introduction

Composite structures are essential in energy absorption, weight reduction, and structure protection. Hence such arrangements received attention for their potential to resolve the instability problem. Various studies have revealed the mechanical behavior of sandwich structures using different techniques, such as using the reinforcement of polymer core materials and functionally graded materials [1-2]. Abud Ali et al. [3] presented a review of the behavior of composite structures. Cellular materials are widely used in nature to build structures that can withstand heavy loads while being lightweight [4]. Industrially, some of the most common engineering utilize cellulosic materials, including those in the aviation and automotive sectors and building and industry packaging; the low density and

excellent stiffness- and strength-to-weight ratios make them ideal for various applications [5]. These cells comprise interconnecting plates or struts that create the cell's borders and faces. The simplest are honeycomb and corrugated, 2D arrays of forms that pack to occupy a planar space, and 3D cellular materials, such as foam, which are used more often [6].

Foams are solid-gas mixtures after manufacture, a cellular solid with many sizes and forms results. High mechanical qualities and low density make foams useful [7]. Open-cell foams are utilized as sound absorbers, filtering, and mattresses. Closed-cell foams are stiffer and used in construction, such as sandwich panels and thermal insulation [8]. Usually, structures include minor faults that differ in size and dispersion based on the material and how it was treated [9]. The structures change depending on cell parameters such as relative density, size, shape, geometrical, wall thickness, and distribution between

struts and faces. Numerous previous studies have revealed the compressive and tensile strength properties of polyurethane foam and polyurethane rigid foam [10]. Maiti et al. (2016) used compressive strain coupled with a time-temperature superposition utilizing a minimum arc length-based method to forecast the long-term performance of the two types of foams [11]. Three-dimensional (3D) printing has recently been highly used to analyze sandwich structures with various applications [12]. 3D printing was explored for creating the lattice cores of these sandwich structures [13]. Lipton and Lipson (2016) presented a method for causing viscous thread instability while implicitly extruding material to produce cellular architectures. Cellular structures manufacture foams for applications ranging from bioengineering to robotics and food printing [14].

Ge et al. (2018) designed cellular structures model that was 3D printed with thermoplastic polyurethane. Flexibility & energy absorption of 3d printed foam were evaluated experimentally [15]. The mechanical behavior of octet-truss microstructures of three distinct octet structures is examined experimentally and numerically by Bagheri et al. [16]. Elasticity modulus increases with increasing strut radius. Results were found to be consistent. Moreover, Guo et al. (2019) presented a new technique to study pyramid lattice core sandwich plates. Theoretical analysis with Hamilton's concept establishes motion's equation. The design of lattice cells will benefit from the new technique [17]. The octahedrons, truncated octahedrons & stellated octahedrons as porous cells are made by selective laser melting. It's experimental, and simulations work. The results indicated that the octahedron configuration has the highest mechanical performance [18].

Lei et al. (2019) created two kinds of multi-layer cores using AlSi10Mg materials, performed numerically and experimentally. Strut position and constructed angle change in strut diameter deviation [19]. Wang et al. (2019) experimental work examine the behavior of sandwich panels with different types of lattice cores using galvanized sheet metal and 3d printed lattice cores. Lattice & graded lattice cores absorb more energy than solids [20]. In their experimental work, Azmi et al. (2019) checked the damage amount & position to see how it affects the natural frequencies of the lattice structure. Increasing damage reduces the natural frequency, and natural frequency values rise as it moves away from the clamped edge [21]. Qi et al. (2020) designed an innovative hybrid sandwich composite of pyramidal truss core reinforced by carbon fiber using finite element models. The study verifies an improvement in the characteristic of the hybrid joining insert [22]. Bonthu et al. (2020) created a 3D-P of a syntactic foam cored sandwich (skin-core-skin printing in sequence at once). This study included optimizing printing conditions and producing high-quality sandwich structures without flaws [23].

Monteiro et al. (2021) found out how sandwich panels' flexural behavior is affected by lattice topology with numerical and experimental methodologies. Relative density constant (0.3). Several lattice geometries have a potential alternative to standard construction [24]. Ma et al. (2021) reported a review study on sandwich panels' features and impact behavior based on cores lattice and

loading conditions as compression. Application and future development have been forecasted [25]. Wei et al. (2021) explored the vibration properties of an octahedral lattice core sandwich, representing theoretical and numerical study. Outcomes coincide perfectly with an octahedron core's natural frequencies by adjusting its cell [26]. Guo et al. (2021) investigated vibration analyses and passive control of sandwiched beams by 3D printed lattice. Theoretical results confirmed empirically, literature findings and simulation showed how 3D printing could create complex lattice cores [27]. The optimal design of core characteristics and skins is also discussed for inhomogeneous [28] and soft polymers [29]. To predict the stability of isotropic composite plates reinforced by different types of powder, Chiad et al. (2020) developed a combined finite element and experimental work [30]. A three-dimensional FEA model predicts the flexural behavior of sandwich structures adhesively bonded to a polymeric foam core consisting of fiber-composite skins (also termed face sheets) [31].

Moreover, studies have been conducted to analyze static and dynamic behaviors of composite structures such as plates and shells [32-34]. Ambreen Kalsoom et al. (2021) investigated the stiffness and damping characteristics of the sandwich beam with 3D printed thermoplastic composite face sheets using higher-order beam theory based on various parameters such as support conditions, non-homogeneous magnetic flux, geometrical properties [35]. Roman Lewandowski et al. (2021) conducted numerical studies on dynamic characteristics for composite sandwich beams made from elastic and viscoelastic layers based on refined zig-zag theory [36]. Al-Waily et al. proposed a dynamic analytical model of the composite plates reinforced with hybrids nanomaterials additives [37]. Studies also focus on static and dynamic experimental works of specific components of the sandwich structure [38]. Recently, many investigations have been proposed to improve the sandwich panel design methods using isotropic face sheets and functionally graded cores. Njim et al. (2021) investigated analytical and numerical investigation of free vibration behavior for sandwich plates with functionally graded porous metal cores and homogenous skins based on classical plate theory [39] and the finite element using the Rayleigh-Ritz [40].

Among the literature on sandwich panels with composite faceplate and foam core, most studies focus on the behavior of core material. However, previous research investigated low-density cellular structures and their application as an alternative to solid materials concentrating on maintaining or improving performance.

The current research includes the experimental and theoretical study of free vibration analysis of a sandwich plate with two sides of aluminum metal and foam core. The study aims to replace the irregular cells foam of the core with a regular cellular structure, where the cells have a standard shape, distribution, and size. Two configurations are employed, one open-cell and the other closed. The theoretical analysis of the two structures is carried out to obtain the free vibration characteristics based on various parameters using mechanical properties obtained from the experimental work. The findings of this study are essential in the automobile industry. The

numerical results presented herein for the cellular core sandwich plate are not available in the literature and hence, should be of interest to future research directions.

I. Structural core

For the structural core to differ from the solid, values of the modulus of elasticity and the poisson ratio, need to be derived as an equation in a different direction. The geometrical structure of cellular solids is defined by the cells' form, size, and distribution. 3D cellular solids like foams have greater complexity than 2D honeycomb structures. But studying two-dimensional structures helps us comprehend three-dimensional structures like foams. The relative density ρ_r of a cellular solid is one of its most essential properties [41],

$$\rho_r = \frac{\rho^*}{\rho_o} \tag{1}$$

Where, ρ^* and ρ_o are the cellular and outer (connected solidly) material densities, respectively. The cell wall thickens with relative density. The outer material's volume fraction is shown in Fig. 1,

$$p_o = \frac{V_o}{V^*} \tag{2}$$

As the density of the foam $\rho^* = \frac{m^*}{V^*}$ and density of the outer material $\rho_o = \frac{m_o}{V_o}$, Since that $m^* = m_o$. The outer material's volume fraction p_o can be written as,

$$p_o = \frac{m_o/\rho_o}{m^*/\rho^*} = \frac{\rho^*}{\rho_o} = \frac{V_o}{V^*} \tag{3}$$

The inner material's relative density matches the outer material's volume fraction $p_i = \frac{V_i}{V^*}$, Also, note that,

$$p_o = \frac{V^* - V_i}{V^*} = 1 - V_i = 1 - \frac{V_i}{V^*} \tag{4}$$

It will seem more like a solid substance with isolated pores if the relative density is more significant than, $p_o > 0.3$.

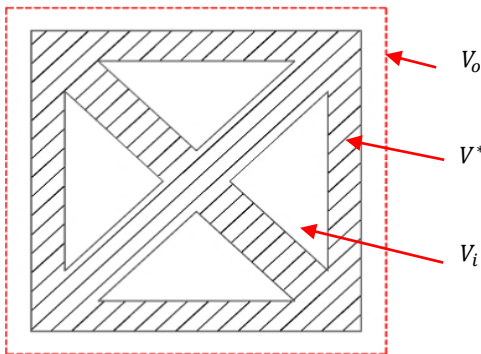


Fig. 1. One cell of cellular structure.

Closed Cell Design

Closed-cell foams have walls, unlike open-cell foams. The proposed for the close cell cubic is symmetric in all

directions, as illustrated in Fig. 2. The way of defining the relative young's modulus is,

$$E_r = \frac{E_c^*}{E_c} \tag{5}$$

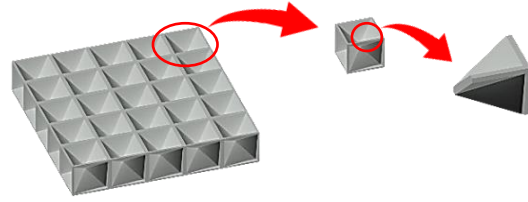


Fig. 2. Closed cell structure.

Where E_c^* and E_c represents Young's modulus of the cellular and solid materials of the closed structure, respectively. The cells are designed to be having same mechanical properties in the x and y directions, as illustrated in Fig. 3. The cell of the foam is symmetric, as shown in Fig. 4, and the characteristics of a rectangular strut with lengths (t) are,

$$\frac{\rho^*}{\rho_o} = 1 - \frac{V_i}{V^*} = 1 - \frac{24V_{is}}{8c^3} = 1 - \frac{3V_{is}}{c^3} \tag{6}$$

$$V_{is} = \frac{1}{3}Ah = \frac{1}{3}(c - t \cos \gamma)^3 \tag{7}$$

So, the final equation would look like this,

$$\frac{\rho^*}{\rho_o} = 1 - \frac{(c - t \cos \gamma)^3}{c^3} \tag{8}$$

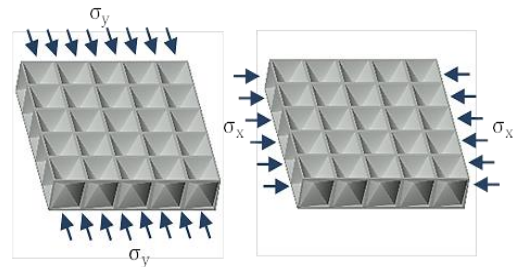


Fig. 3. Closed-cell in x-y direction to conclude young's modulus.

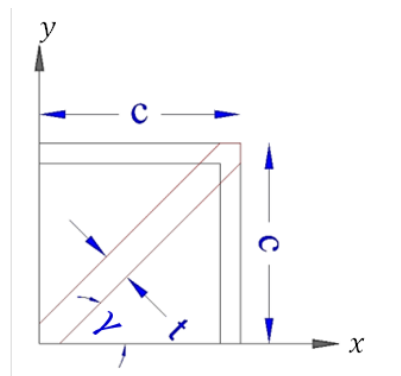


Fig. 4. The closed-cell area (eighth cells).

Modeled an isotropic closed-cell foam and provided an estimated foam Young's modulus linked to the solid

Young's modulus as a function of the proportion of solid material in struts φ by [8],

$$\frac{E_c^*}{E_c} \approx C_1 \varphi^2 \left(\frac{\rho^*}{\rho_0} \right)^2 + C_1' (1 - \varphi) \frac{\rho^*}{\rho_0} + \frac{p_{at}(1-2\nu^*)}{E_0(1-\frac{\rho^*}{\rho_0})} \quad (9)$$

$$G_c^* = \frac{E_f^*}{2(1+\nu_f^*)} \quad (10)$$

$C_1 \approx C_1' \approx 1$ and the last term in Eq. (9) can be neglected as it almost equals zero, also atmospheric pressure $p_{at} = 0.1$ Mpa, then the equation goes,

$$\frac{E_c^*}{E_c} \approx \varphi^2 \left(\frac{\rho^*}{\rho_0} \right)^2 + (1 - \varphi) \frac{\rho^*}{\rho_0} \quad (11)$$

By substitution Eq. (8) in Eq. (11), get,

$$\frac{E_c^*}{E_c} \approx \left(\varphi^2 \left(1 - \frac{(c-t \cos \gamma)^3}{c^3} \right)^2 + (1 - \varphi) \left(1 - \frac{(c-t \cos \gamma)^3}{c^3} \right) \right) \quad (12)$$

And since the cell is symmetrical in the x and y direction then, the equation becomes,

$$E_{c2}^* = E_{c1}^* = E_c^* = \left(\varphi^2 \left(1 - \frac{(c-t \cos \gamma)^3}{c^3} \right)^2 + (1 - \varphi) \left(1 - \frac{(c-t \cos \gamma)^3}{c^3} \right) \right) E_c \quad (13)$$

Percentage of the strut from the total material forming the solid part of the core structure (φ). To obtain the following equation, the free vibration equation was derived based on Kirchhoff's theory of a three-layer sandwich plate (two faces of plates and a core) [42, 43],

$$\omega_{mn} = \sqrt{\frac{\left(\frac{\pi}{a} \right)^4 \left(2 \left(\frac{2E_s}{1-\nu_s^2} \left(\frac{h_s^3}{3} + \frac{h_s^2 h_f}{2} + \frac{h_s h_f^2}{4} \right) + \frac{E_f}{1-\nu_f^2} \left(\frac{h_f^3}{12} \right) \right) + \left(\frac{4E_s}{(1+\nu_s)} \left(\frac{h_s^3}{3} + \frac{h_s^2 h_f}{2} + \frac{h_s h_f^2}{4} \right) + G_f \left(\frac{h_f^3}{3} \right) \right)}{2\rho_s h_s + \rho_f h_f}} \quad (14)$$

The new modified equation, instead of after the back substitution of the equations,

$$\omega_{mn} = \sqrt{\frac{\left(\frac{\pi}{a} \right)^4 \left(2 \left(\frac{2E_s}{1-\nu_s^2} \left(\frac{h_s^3}{3} + \frac{h_s^2 h_f}{2} + \frac{h_s h_f^2}{4} \right) + \frac{E_c^*}{1-\nu_c^2} \left(\frac{h_f^3}{12} \right) \right) + \left(\frac{4E_s}{(1+\nu_s)} \left(\frac{h_s^3}{3} + \frac{h_s^2 h_f}{2} + \frac{h_s h_f^2}{4} \right) + G_c^* \left(\frac{h_f^3}{3} \right) \right)}{2\rho_s h_s + \rho_f^* h_f}} \quad (15)$$

Open Cell Design

Most open-cell foams lack walls. Procedures remove cell membranes physically or chemically. Applying the same approach for open cells, proposing cell cubic symmetric in two directions as illustrated in Fig. 5. They were using the same equation only by adopting mechanical properties for open-cell. The same way in defining relative young's modulus as mechanical the same in x and y directions as illustrated in Fig. 6. As shown in Fig. 7, the chosen open cell has three areas,

$$\frac{\rho^*}{\rho_0} = \frac{V_0}{V^*} = \frac{4(V_{os})}{4c^2 h} = \frac{V_{os}}{c^2 h} \quad (16)$$

$$V_{os} = \left(t \left(\left(c^2 - \left(c - \frac{t}{2} \right) \right) + (c^2 - (c - t)) \right) + t^2 \left(\sqrt{2c^2 + (h - 2t)^2} - \frac{t}{\tan \gamma} \right) \right) \quad (17)$$

So, the final equation is going to be,

$$\frac{\rho^*}{\rho_0} = \frac{1}{c^2 h} \left(t \left(\left(c^2 - \left(c - \frac{t}{2} \right) \right) + (c^2 - (c - t)) \right) + t^2 \left(\sqrt{2c^2 + (h - 2t)^2} - \frac{t}{\tan \gamma} \right) \right) \quad (18)$$

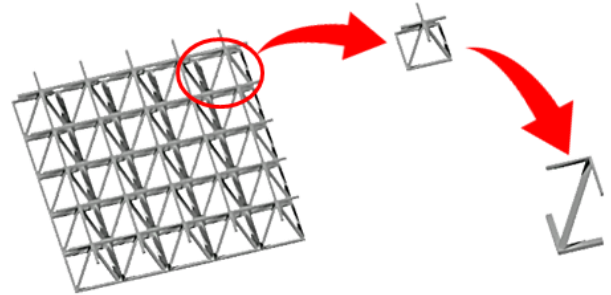


Fig. 5. The open cell structure.

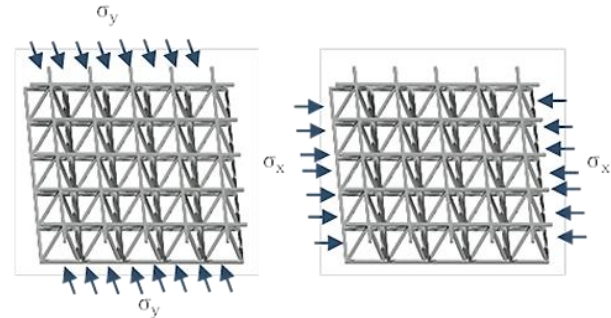
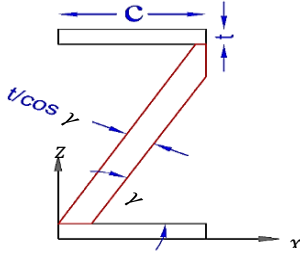


Fig. 6. Open the cell in the x-y direction to conclude young's modulus.


Fig. 7. closed-cell (quarter cell).

As a result, [8] calculated the open-cell foam's elastic constants using the cubic model,

$$\frac{E_c^*}{E_c} \approx C_1 \left(\frac{\rho^*}{\rho_0} \right)^2 \quad (19)$$

$$G_c^* = \frac{E_f^*}{2(1+\nu_f^*)} \quad (20)$$

As $C_1 \approx 1$ and $\nu^* = 0.3$, the equation goes,

$$\frac{G_c^*}{E_c} \approx \frac{3}{8} \left(\frac{\rho^*}{\rho_0} \right)^2 \quad (21)$$

$$\frac{E_c^*}{E_c} \approx \left(\frac{1}{c^2 h} \left(t \left(\left(c^2 - \left(c - \frac{t}{2} \right) \right) + \left[c^2 - (c-t) \right] \right) + t^2 \left(\sqrt{2c^2 + (h-2t)^2} - \frac{t}{\tan \gamma} \right) \right) \right)^2 \quad (22)$$

And since the cell is symmetrical in the x and y direction then, the equation becomes,

$$E_{c2}^* = E_{c1}^* = E_c^* = \left(\frac{1}{c^2 h} \left(t \left(\left(c^2 - \left(c - \frac{t}{2} \right) \right) + \left(c^2 - (c-t) \right) \right) + t^2 \left(\sqrt{2c^2 + (h-2t)^2} - \frac{t}{\tan \gamma} \right) \right) \right)^2 E_c \quad (23)$$

Using the same equations (14) and (15) to compute for the natural frequency.

II. Results

For a rectangular sandwich plate, $a = b = 30\text{cm}$. Using two Faces with a thickness of $h_s = 1\text{mm}$ of aluminum alloy (Al 1100-H12) has $E_s = 68.9\text{ Gpa}$, $\rho_s = 2710\text{ kg/m}^3$ & $\nu_s = 0.33$. The core part with a thickness of $h_f = 14\text{mm}$. The material to be adopted in the core structure is polylactic acid (PLA) and Thermoplastic polyurethane (TPU). The tensile test is carried out to find mechanical properties according to ASTM. Hence, standard specimens for PLA and TPU material are used as raw materials in 3D printing machines to make structural foam, depending on ASTM D638 for plastic materials [44, 45]. Two types of samples adopted rigid and non-rigid plastic specimens for the record, as illustrated in Fig. 8. According to the standards, five samples of each material, with the dimensions listed in Table 1.

Table 1.

ASTM D638 for plastic rigid (PLA) and non-rigid (TPU).

Measurements	PLA (mm)	TPU (mm)
Lo	165	115
L	33	20
Wo	20	19
W	12.5	6
R	76	14
Ri	-	25
Thickness	3	3
Gauge length	50	25

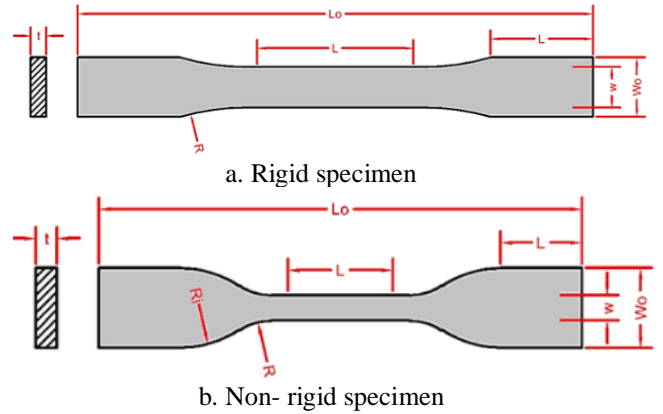

Fig. 8. ASTM D638 specimens.

Table 2.

Printing parameters of all specimens.

Printing setting	PLA filament	TPU filament
Nozzle dia.	0.40mm	0.50mm
Layer thickness	0.28mm	0.25mm
Infilling density	100%	100%
Infilling pattern	lines	lines
Printing temp.	200° C	228° C
Bed temp.	60° C	65° C
Printing speed	50mm/sec.	25mm/sec.

As the average results, PLA has a young's modulus magnitude of 1.175 Gpa and a density of 1360 kg/m³, while TPU has a young's modulus magnitude of 0.833 Gpa and a density of 1450 kg/m³. Printed specimens are illustrated in Fig. 9 before and after testing. First,

choose the cell dimension to build the core for open and closed cells. The selected cell is cubic in shape with a length of 14mm. The other dimension to be calculated like strut thickness, with a critical relative density as $\rho_r > 0.3$. Table 3 shows the selected strut thickness results as well as the calculated young modulus. In comparison with PLA, the stiffness of TPU polymer type decreases with thickness.

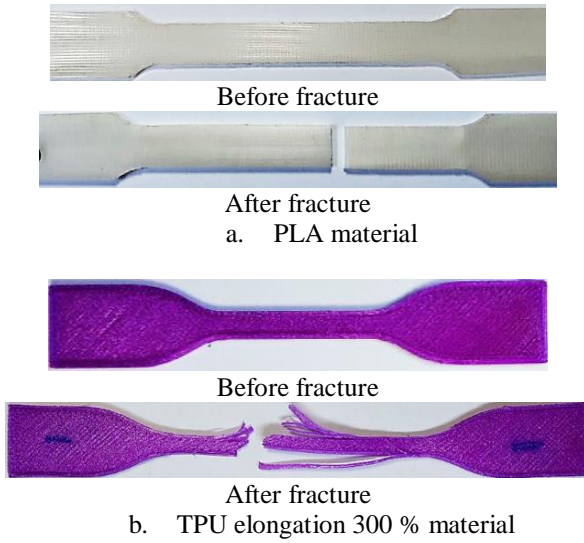


Fig. 9. Tensile specimen before and after testing .

As can be seen from the results, the fundamental natural frequency increases as a function of relative

density. Table 4 compares the natural frequency results between the traditional shape with open and closed cells at h_c 0.014 (m). Based on the results, it is evident that the new design has a distinct improvement in natural frequency. According to Table 5, closed-cell designs adopting varying strut thicknesses produce different results. According to the table, natural frequency and Young modulus increase as the proportion of solid material in struts ϕ decreases, furthermore the PLA samples showing significantly higher stiffness than TPU samples.

The natural frequency to elasticity modulus relation is illustrated in Fig. 10 for open cells and Fig. 11 for closed cells, while the connection to relative density is presented in Fig. 12 for available cells and Fig. 13 for closed cells. Fig. 14 shows the strut thickness effect on the natural frequency.

III. Discussion

With the Derivation of equations for extracting and converting mechanical properties from relative density, Young's modulus, stiffness modulus, and Poisson ratio. Relying on the equation for extracting the natural frequency, we discuss the results as follows,

Figures (10) and (11) show the relationship between the natural frequency and the modulus of elasticity. The connection is inverse with the decrease in the modulus of elasticity, so the natural frequency increases, and this decrease comes after converting the solid material into

Table 3.

Open cell design results adopting varying strut thickness ranges							
Mat	t, mm	ρ_r	E_c^* , Gpa	v_c^*	G_c^* , Gpa	ρ_c^* , kg/m ³	ω , rad/sec
PLA	1.1	0.163	0.031	0.3	0.012	222.21	6046.38
	1.2	0.181	0.038	0.3	0.015	245.68	5933.88
	1.3	0.198	0.046	0.3	0.018	269.59	5825.61
	1.4	0.216	0.055	0.3	0.021	293.91	5721.44
	1.5	0.234	0.064	0.3	0.025	318.64	5621.23
	1.6	0.253	0.075	0.3	0.029	343.73	5524.85
	1.7	0.271	0.087	0.3	0.033	369.17	5432.16
	1.8	0.290	0.099	0.3	0.038	394.94	5343.01
	1.9	0.310	0.113	0.3	0.043	421.02	5257.27
	2	0.329	0.127	0.3	0.049	447.38	5174.80
TPU	1.1	0.163	0.022	0.3	0.009	236.91	5973.81
	1.2	0.181	0.027	0.3	0.010	261.93	5858.01
	1.3	0.198	0.033	0.3	0.013	287.43	5746.78
	1.4	0.216	0.039	0.3	0.015	313.36	5639.96
	1.5	0.234	0.046	0.3	0.018	339.72	5537.38
	1.6	0.253	0.053	0.3	0.020	366.48	5438.88
	1.7	0.271	0.061	0.3	0.024	393.60	5344.27
	1.8	0.290	0.070	0.3	0.027	421.08	5253.41
	1.9	0.310	0.080	0.3	0.031	448.88	5166.13
	2	0.329	0.090	0.3	0.035	476.99	5082.28

Table 4.

Comparison the result of the traditional shape with the open and closed cells at h_c 0.014 (m).						
Mat.	E_c^* , Gpa	ρ_s (kg/m ³)	ρ_r	vc	ρ_c (kg/m ³)	ω (rad/s)
PLA	1.175	1360	1	0.38	1360	5239.38
TPU	0.833	1450	1	0.35	1450	5080.74

Table 5.

Closed-cell design results adopting varying strut thickness

Mat	t mm	φ	ρ_r	E_c^* Gpa	ν_c^*	G_c^* Gpa	ρ_c^* kg/m ³	ω rad/sec
PLA	1.1	0.22	0.298	0.236	0.3	0.091	404.85	5321.43
	1.2	0.24	0.321	0.249	0.3	0.096	437.04	5217.62
	1.3	0.26	0.344	0.262	0.3	0.101	468.51	5121.86
	1.4	0.28	0.367	0.274	0.3	0.105	499.25	5033.24
	1.5	0.30	0.389	0.285	0.3	0.110	529.27	4951.00
	1.6	0.32	0.411	0.296	0.3	0.114	558.59	4874.48
	1.7	0.34	0.432	0.305	0.3	0.117	587.21	4803.14
	1.8	0.36	0.452	0.315	0.3	0.121	615.14	4736.48
	1.9	0.38	0.472	0.324	0.3	0.125	642.39	4674.07
	2	0.40	0.492	0.333	0.3	0.128	668.97	4615.55
TPU	1.1	0.22	0.298	0.236	0.3	0.091	431.64	5233.64
	1.2	0.24	0.321	0.249	0.3	0.096	465.96	5128.41
	1.3	0.26	0.344	0.262	0.3	0.101	499.51	5031.51
	1.4	0.28	0.367	0.274	0.3	0.105	532.28	4941.98
	1.5	0.30	0.389	0.285	0.3	0.110	564.30	4859.01
	1.6	0.32	0.411	0.296	0.3	0.114	595.56	4781.93
	1.7	0.34	0.432	0.305	0.3	0.117	626.07	4710.13
	1.8	0.36	0.452	0.315	0.3	0.121	655.85	4643.12
	1.9	0.38	0.472	0.324	0.3	0.125	684.90	4580.46
	2	0.40	0.492	0.333	0.3	0.128	713.24	4521.75

foam that permeates every air cell, as seen in fig. (12) and (13). The difference between the rigid material (PLA) and the non-rigid (TPU) is evident as the tough material comes at a higher frequency.

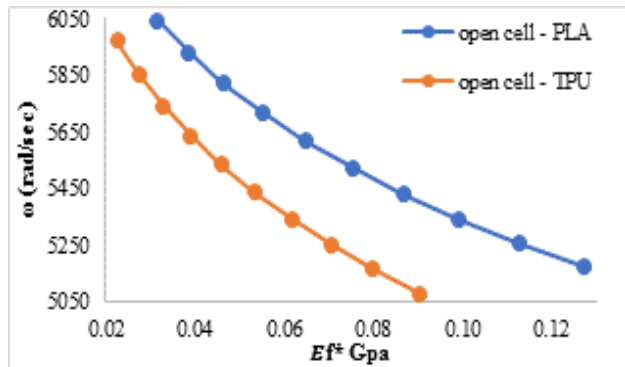


Fig. 10. Natural frequency to elasticity modulus for open cell.

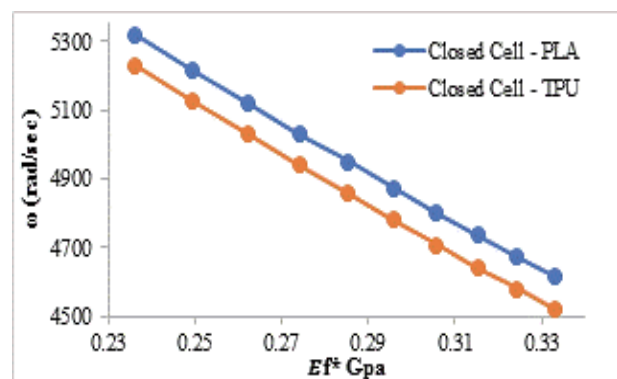


Fig. 11. Natural frequency to elasticity modulus for closed cell.

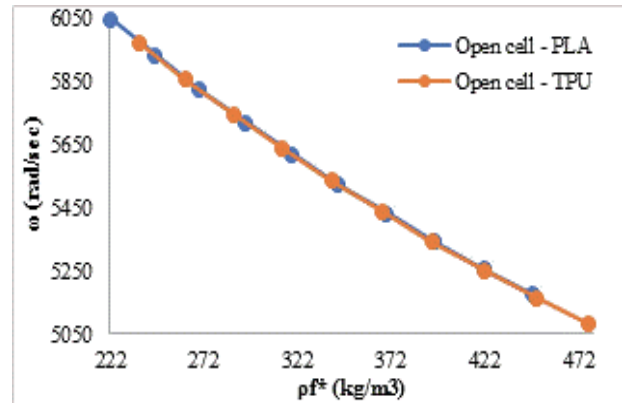


Fig. 12. Natural frequency to relative density for open cell.

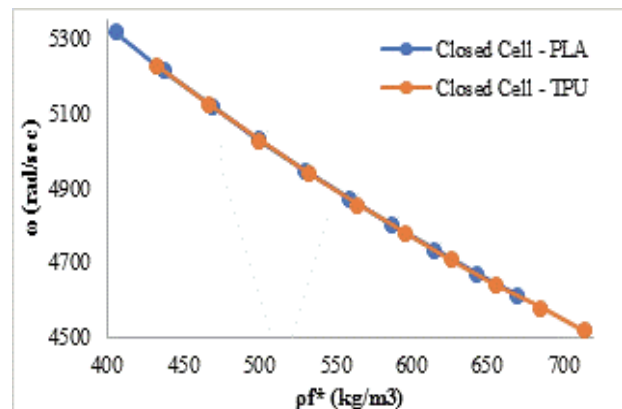


Fig. 13. Natural frequency relation relative density for closed-cell.

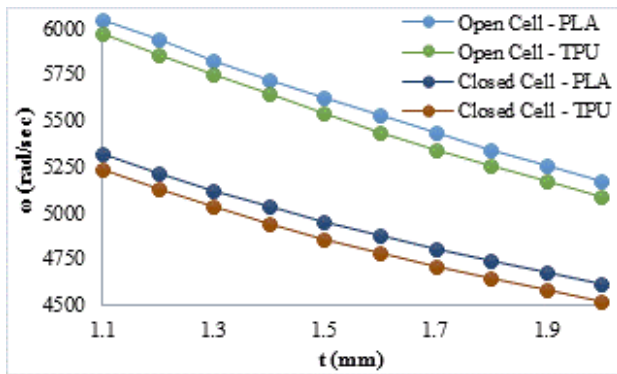


Fig. 14. Natural frequency to strut thickness with two cell types (Open & Closed) and two materials (PLA & TPU).

For open lattice cells, depending on the relative density as a regulator. When the relative density (0.3) at ($t = 1.9\text{mm}$) compared to solid matter, the percentage decrease in the modulus of elasticity by (PLA: -90.4%) and (TPU: -90.4%), increases the natural frequency by (PLA: 44.5%) and (TPU: 46.4%). One more time, a closed lattice cell with the same relative density (0.3) at ($t = 1.5\text{mm}$) compared to solid matter. Percentage decrease in the modulus of elasticity by (PLA: -66.9%) and (TPU: -64.4%) increases the natural frequency by (PLA: 36%) and (TPU: 37.7%). Converting a solid material into a cellular one to reduce weight loses some properties. The properties can be compensated by adding a nanomaterial or by filling the cellular part with another material and turning it into a hybrid structure.

Conclusions

After reviewing the results in tables and charts and discussing the results as in the previous text, the following is concluded,

The effect of converting a solid material or replacing a foam form with a cellular pattern is very effective.

The choice of cell shape and pattern determines their performance. The regular shape in both directions makes the material isotropic and homogeneous

Selection between closed and open-cell depends on the application, and it is preferable to use a closed-cell in the sandwich because it offers much performance.

The open-cell structure can be converted into a closed one by filling the attached space with another material, such as foam, which makes the core a hybrid shape that offers the performance the engineer aspires to.

Effectiveness of cellular pattern theoretical analysis estimation and possible use in various applications

The results of this investigation can be used in various engineering applications such as retractable car roofs, the floor of electric cars to isolate the cabin from the battery placed under the vehicle, and electric motor covers for electric cars.

Nomenclature

Symbols	Definition
a	Plate length in x-direct (m)
b	Plate width in y-direct (m)
c	Half of the cell length or width (m)
E_s	face layer young's modulus (Pa)
E_f	core layer young's modulus (Pa)
E_c^*	cellular core material young's modulus (Pa)
E_c	solid material young's modulus (Pa)
G_f	core layer rigidity modulus (Pa)
G_c^*	cellular core layer rigidity modulus (Pa)
h_s	Upper face layer height (m)
h_f	lower face layer height (m)
p_i	Inner volume fraction
p_o	Outer volume fraction
t	The thickness of the cell frame (m)
V^*	cellular material Volume (m^3)
V_o	outer (connected solid) material Volume (m^3)
V_i	inner (air) Volume (m^3)
V_{is}	Inner air volume (m^3)
V_{os}	Outer frame volume (m^3)
ω_{mn}	Natural frequency (rad/s)
ν_s	face layer Poisson's ratio
ν_c^*	cellular Poisson's ratio
ρ_r	Relative density
ρ^*	cellular material density (kg/m^3)
ρ_f	face layer density (kg/m^3)
ρ_s	core layer density (kg/m^3)
ρ_o	outer (connected solid) material density (kg/m^3)
φ	the proportion of solid material in struts

Hussam Raad – M.Sc. researcher (Applied Mechanics) raadhussam4@gmail.com;

Emad Kadum Njim – Ph.D. researcher (Applied Mechanics) emad.njim@gmail.com;

Muhsin J. Jweeg – Prof. Dr. (Applied Mechanics) muhsinjj@gmail.com;

Muhannad Al-Waily – Prof. Dr. (Applied Mechanics) muhanedl.alwaeli@uokufa.edu.iq.

- [1] E.K. Njim, S.H. Bakhy, M. Al-Waily, *Analytical and numerical flexural properties of polymeric porous functionally graded (PFGM) sandwich beams*, Journal of Achievements in Materials and Manufacturing Engineering 110 (1), 5 (2022); <https://doi.org/10.5604/01.3001.0015.7026>.
- [2] E.K. Njim, S.H. Bakhy, M. Al-Waily, *Free vibration analysis of imperfect functionally graded sandwich plates: analytical and experimental investigation*, Archives of Materials Science and Engineering 111 (2), 49 (2021); <https://doi.org/10.5604/01.3001.0015.5805>.
- [3] ZAA Abud Ali, A.A. Kadhim, R.H. Al-Khayat, M. Al-Waily, *Review Influence of Loads upon Delamination Buckling in Composite Structures*, Journal of Mechanical Engineering Research and Developments 44 (3), 392 (2021).

- [4] A. Öchsner, G.E. Murch, M.J.S. de Lemos, *Cellular and Porous Materials: Thermal Properties Simulation and Prediction*, Wiley-VCH Verlag GmbH & Co. KgaA (2008).
- [5] A. Karakoç, *Effective stiffness and strength properties of cellular materials in the transverse plane*, Aalto University publication series (2013). <https://doi.org/10.1002/9783527621408>.
- [6] L.J. Gibson, M. F. Ashby, *Cellular solids: Structure and properties*, second edition, Lorna J. Gibson and Michael F. Ashby (1997).
- [7] P. Stevenson, *Foam Engineering: Fundamentals and Applications*, John Wiley & Sons (2012).
- [8] V. Shulmeister, *Modelling of the Mechanical Properties of Low-Density Foams*, Shaker (1997).
- [9] H. Altenbach, A. Öchsner, *Cellular and Porous Materials in Structures and Processes*, Springer Nature Switzerland AG (2012). <https://doi.org/10.1007/978-3-7091-0297-8>.
- [10] A. Koyama, D. Suetsugu, Y. Fukubayashi, H. Mitabe, *Experimental study on the dynamic properties of rigid polyurethane foam in stress-controlled cyclic uniaxial tests*, *Construction and Building Materials*, 321(2022); <https://doi.org/10.1016/j.conbuildmat.2022.126377>.
- [11] A. Maiti, W. Small, J.P Lewicki, T.H. Weisgraber, E.B. Duoss, S.C. Chinn, *3D printed cellular solid outperforms traditional stochastic foam in long-term mechanical response*, *Scientific Reports* 6 (2016); <https://doi.org/10.1038/srep24871>.
- [12] E.K. Njim, S.H. Bakhy, M. Al-Waily, *Experimental and numerical flexural analysis of porous functionally graded beams reinforced by (Al/Al₂O₃) nanoparticles*, *International Journal of Nanoelectronics and Materials* 15 (2), 94 (2022).
- [13] A. Fadeel, H. Abdulhadi, G. Newaz, R. Srinivasan, A. Mian, *Computational investigation of the post-yielding behavior of 3D-printed polymer lattice structures*, In *Journal of Computational Design and Engineering*, 9 (1), 263 (2022), <https://doi.org/10.1093/jcde/qwac001>.
- [14] J.I. Lipton, H. Lipson, *3D Printing Variable Stiffness Foams Using Viscous Thread Instability*, *Scientific Reports* 6 (2016).
- [15] C. Ge, L. Priyadarshini, D. Cormier, L. Pan, J. Tuber, *A preliminary study of cushion properties of a 3D printed thermoplastic polyurethane Kelvin foam*, *Packaging Technology and Science* 31(5) (2018); <https://doi.org/10.1002/pts.2330>.
- [16] A. Bagheri, I.B. Corral, M. Ferrer, M.M. Pastor, F. Roure, *Determination of the elasticity modulus of 3D printed octet-truss structures for use in porous prosthesis implants*, *Materials* 11(12), (2018) <https://doi.org/10.3390/ma11122420>.
- [17] Z. Guo, C. Liu, F. Li, *Vibration analysis of sandwich plates with lattice truss core*, *Mechanics of Advanced Materials and Structures*, 26(5) (2019); <https://doi.org/10.1080/15376494.2017.1400616>.
- [18] C. Tian, X. Li, S. Zhang, G. Guo, S. Ziegler, J.H. Schleifenbaum, *Porous structure design and fabrication of metal-bonded diamond grinding wheel based on selective laser melting (SLM)*, *International Journal of Advanced Manufacturing Technology*. 100 (5–8) (2019); <https://doi.org/10.1007/s00170-018-2734-y>.
- [19] H. Lei, C. Li, J. Meng, H. Zhou, Y. Liu, X. Zhang, *Evaluation of compressive properties of SLM-fabricated multi-layer lattice structures by experimental test and μ -CT-based finite element analysis*, *Materials and Design* 169 (2019). <https://doi.org/10.1016/j.matdes.2019.107685>.
- [20] S. Wang, Y. Xu, W. Zhang, *Low-velocity impact response of 3D-printed lattice sandwich panels*, *IOP Conference Series: Materials Science and Engineering* 531 (2019).
- [21] MS Azmi, R. Ismail, R. Hasan, A. Putra, M.N. Nurdin, *Effect of damage on FDM printed lattice structure material vibration characteristics*, *Proceedings of Mechanical Engineering Research Day* (2019).
- [22] G. Qi, Y.L. Chen, P. Richert, L. Ma, K.U. Schröder, *A hybrid joining insert for sandwich panels with pyramidal lattice truss cores*, *Composite Structures* 241 (2020); <https://doi.org/10.1016/j.compstruct.2020.112123>.
- [23] D. Bonthu, H.S. Bharath, S. Gururaja, P. Prabhakar, M. Doddamani, *3D printing of syntactic foam cored sandwich composite*, *Composites Part C: Open Access* 3 (2020); <https://doi.org/10.1016/j.jcomc.2020.100068>.
- [24] J.G. Monteiro, M. Sardinha, F. Alves, A.R. Ribeiro, L. Reis, A. M. Deus, *Evaluation of the effect of core lattice topology on the properties of sandwich panels produced by additive manufacturing*, *Proceedings of the Institution of Mechanical Engineers, Part L: Journal of Materials: Design and Applications* 235 (6) (2021); <https://doi.org/10.1177/1464420720958015>.
- [25] Q. Ma, M.R.M. Rejab, J.P. Siregar, Z. Guan, *A review of the recent trends on core structures and impact response of sandwich panels*, *Journal of Composite Materials* 55 (18) (2021); <https://doi.org/10.1177/0021998321990734>.
- [26] N. Wei, H. Ye, X. Zhang, J. Li, B. Yuan, *Vibration Characteristics Research of Sandwich Structure with Octet-truss Lattice Core*, *Journal of Physics: Conference Series* 2125 (1) (2021); <https://iopscience.iop.org/article/10.1088/1742-6596/2125/1/012059>.
- [27] Z. Guo, G. Hu, J. Jiang, L. Yu, X. Li, J. Liang, *Theoretical and Experimental Study of the Vibration Dynamics of a 3D-Printed Sandwich Beam With an Hourglass Lattice Truss Core*, *Front Mech Eng*, 7 (2021); <https://doi.org/10.3389/fmech.2021.651998>.
- [28] E.K. Njim, S.H. Bakhy, M. Al-Waily, *Optimisation Design of Functionally Graded Sandwich Plate with Porous Metal Core for Buckling Characterisations*, *Pertanika Journal of Science & Technology*, 29(4), 3113 (2021); <https://doi.org/10.47836/pjst.29.4.47>.

- [29] E.K. Njim, S.H. Bakhy, M. Al-Waily, *Optimization design of vibration characterizations for functionally graded porous metal sandwich plate structure*, *Materials Today: Proceedings* (2021); <https://doi.org/10.1016/j.matpr.2021.03.235>.
- [30] J.S. Chiad, M. Al-Waily, M.A. Al-Shammari, *Buckling Investigation of Isotropic Composite Plate Reinforced by Different Types of Powders*, *International Journal of Mechanical Engineering and Technology* 9 (9), 305 (2018).
- [31] H. Liu, J. Liu, Ci. Kaboglu, J. Zhou, Xi.o Kong, Sh. Li, B. R.K. Blackman, A. J. Kinloch, J. P. Dear, *Modelling the quasi-static flexural behaviour of composite sandwich structures with uniform- and graded-density foam cores*, *Engineering Fracture Mechanics*, 259 (2022); <https://doi.org/10.1016/j.engfracmech.2021.108121>.
- [32] M. Al-Waily, A.M. Jaafar, *Energy balance modelling of high velocity impact effect on composite plate structures*, *Archives of Materials Science and Engineering*, 111(1), 14 (2021).
- [33] E.N. Abbas, M.J. Jweeg, M. Al-Waily, *Analytical and Numerical Investigations for Dynamic Response of Composite Plates Under Various Dynamic Loading with the Influence of Carbon Multi-Wall Tube Nano Materials*, *International Journal of Mechanical & Mechatronics Engineering*, 18(6), 1 (2018).
- [34] M. Al-Waily, M.A. Al-Shammari, M.J. Jweeg, *An Analytical Investigation of Thermal Buckling Behavior of Composite Plates Reinforced by Carbon Nano Particles*, *Engineering Journal* 24(3) (2020); <https://doi.org/10.4186/ej.2020.24.3.11>.
- [35] A. Kalsoom, A. N. Shankar, I. Kakaravada, P. Jindal, V. V. K. Lakshmi, and S. Rajeshkumar, *Investigation of dynamic properties of a three-dimensional printed thermoplastic composite beam containing controllable core under non-uniform magnetic fields*, *Journal of Materials: Design and Applications.*; 236 (2), 404 (2021) <https://doi.org/10.1177/146442072111045943>.
- [36] R. Lewandowski, P. Litewka, P. Wielentejczyk, *Free vibrations of laminate plates with viscoelastic layers using the refined zig-zag theory – Part I. Theoretical background*, *Composite Structures*, 278, (2021); <https://doi.org/10.1016/j.compstruct.2021.114547>.
- [37] M. Al-Waily, M.J. Jweeg, M.A. Al-Shammari, K.K. Resan, A.M. Takhakh, *Improvement of Buckling Behavior of Composite Plates Reinforced with Hybrids Nanomaterials Additives*, *Materials Science Forum* 1039 23 (2021);
- [38] E.K. Njim, M. Al-Waily, S.H. Bakhy, *A Review of the Recent Research on the Experimental Tests of Functionally Graded Sandwich Panels*, *Journal of Mechanical Engineering Research and Developments* 44(3), 420 (2021).
- [39] E.K. Njim, S.H. Bakhy, M. Al-Waily, *Analytical and Numerical Investigation of Free Vibration Behavior for Sandwich Plate with Functionally Graded Porous Metal Core*, *Pertanika Journal of Science & Technology* 29(3), 1655 (2021); <https://doi.org/10.47836/pjst.29.3.39>.
- [40] E. K. Njim, S. H. Bakhy, M. Al-Waily, *Analytical and numerical free vibration analysis of porous functionally graded materials (FGPMs) sandwich plate using Rayleigh-Ritz method*, *Archives of Materials Science and Engineering* 110 (1), 27 (2021); <https://doi.org/10.5604/01.3001.0015.3593>.
- [41] D. Lukkassen A. Meidell, *Advanced materials and structures and their fabrication processes*, Book manuscript, Narvik University College, HiN 2 (2007).
- [42] S.S. Rao, *Vibration of continuous systems*, John Wiley & Sons, Inc. (2019).
- [43] A.W. Leissa, *Vibration of Plates*, NASA, Washington, DC (1984).
- [44] E. K. Njim, S. H. Bakhy, M. Al-Waily, *Analytical and numerical investigation of buckling load of functionally graded materials with porous metal of sandwich plate*, *Materials Today: Proceedings* (2021); <https://doi.org/10.1016/j.matpr.2021.03.557>.
- [45] E.K. Njim, S.H. Bakhy, M. Al-Waily, *Analytical and Numerical Investigation of Buckling Behavior of Functionally Graded Sandwich Plate with Porous Core*, *Journal of Applied Science and Engineering*. 25(2), 339 (2022); [http://dx.doi.org/10.6180/jase.202204_25\(2\).0010](http://dx.doi.org/10.6180/jase.202204_25(2).0010).

Аналіз вібрації багат шарової пластини із відкритою та закритою комірками

¹Кафедра механічної інженерії, інженерний факультет, університет Куфи, Ірак

²Міністерство промисловості та мінералів, Державна компанія виробництва гуми та шин, Ірак

³Університет Аль-Фарахіді, коледж технічної інженерії, Ірак

У роботі здійснено спробу замінити традиційну форму та матеріал серцевини сендвіча стільниковою формою, у якій клітини мають правильні форму, розподіл та розмір. Ідея цієї статті полягає в розробці двох структур, одна із яких з відкритою коміркою, а інша із закритою, а також в оцінці ефективності сендвіч-пластини із ґратковою коміркою серцевини, що використовується для багатьох промислових застосувань, зокрема в автомобілебудуванні. Нові теоретичні формулювання побудовані для двох структур для знаходження характеристик вільних коливань. Результати такої моделі порівнюються із традиційною формою. Виведені рівняння для прогнозування механічних властивостей на основі відносної густини з вибраними формами, специфічне рівняння вібрації тришарової сендвіч-плити та розв'язано за допомогою таблиць Excel. Багатообіцяючими є результати, і оцінка ефективності теоретичного аналізу клітинної структури. Обмеження та частота похибок для механічних властивостей впливають з емпіричних рівнянь, і їх співвідношення до значень відносної густини є вищим залежно від поведінки матеріалу серцевини. Висновки вказують, що при відкритих комірках спостерігається зниження модуля пружності на (PLA: -90,4%) і (TPU: -90,4%) та збільшення власної частоти на (PLA: 44,5%) і (TPU: 46,4%), тоді як для закритих комірок модуль пружності зменшується на (PLA: -66,9%) і (TPU: -64,4%), а також збільшується власна частота на (PLA: 36%) і (TPU: 37,7%). Перетворення твердої речовини або заміна пінопластової форми стільниковою формою є одним із способів покращити продуктивність і заощадити вагу завдяки вибраній стільниковій конфігурації при поглинанні енергії вібраційної хвилі.

Ключові слова: сендвіч-плита, вільні коливання, конструкція комірки, розпірна секція, закриті та відкриті комірки, відносна щільність.